Received: 1 November 2018 | Revised: 14 December 2018 | Accepted: 18 December 2018

DOI: 10.1002/chir.23056

REGULAR ARTICLE

WILEY

Circularly polarized luminescence of Sm (III) and Eu (III) complexes with chiral ligand (*R*/*S*)-BINAPO

Daniel Cotter | Spencer Dodder | Valentine J. Klimkowski | Todd A. Hopkins

Department of Chemistry and Biochemistry, Butler University, Indianapolis, Indiana

Correspondence
Todd A. Hopkins, Department of Chemistry and Biochemistry, Butler University, 4600 Sunset Avenue, Indianapolis, IN 46208.
Email: tahopkin@butler.edu

Funding information
Butler Program for Undergraduate Research

Abstract

Luminescent lanthanide (III) ions have been exploited for circularly polarized luminescence (CPL) for decades. However, very few of these studies have involved chiral samarium (III) complexes. Complexes are prepared by mixing axial chiral ligands (*R*/*S*))-2,2'-bis(diphenylphosphoryl)-1,1′-binaphthyl (BINAPO) with europium and samarium Tris (trifluoromethane sulfonate) (Eu $(OTf)_3$ and Sm $(OTf)_3$). Luminescence-based titration shows that the complex formed is Ln((*R*/*S*)-BINAPO)$_2$(OTf)$_3$, where Ln = Eu or Sm. The CPL spectra are reported for Eu((*R*/*S*)-BINAPO)$_2$(OTf)$_3$ and Sm((*R*/*S*)-BINAPO)$_2$(OTf)$_3$. The sign of the dissymmetry factors, g_{em}, was dependent upon the chirality of the BINAPO ligand, and the magnitudes were relatively large. Of all of the complexes in this study, Sm((*S*)-BINAPO)$_2$(OTf)$_3$ has the largest g_{em} = 0.272, which is one of the largest recorded for a chiral Sm^{3+} complex. A theoretical three-dimensional structural model of the complex that is consistent with the experimental observations is developed and refined. This report also shows that (*R*/*S*)-BINAPO are the only reported ligands where g_{em} (Sm^{3+}) > g_{em} (Eu^{3+}).

KEYWORDS

BINAPO, circularly polarized luminescence, europium, samarium

1 | INTRODUCTION

Circularly polarized luminescent materials have potential application in the development of three-dimensional displays,[1] information storage,[2] and as probes of biomolecular processes.[3,4] This has led to the development of a number of circularly polarized luminescent molecules including organic dyes,[5-10] helicenes,[7,11-14] and transition metal complexes.[15-17] However, chiral complexes of luminescent lanthanide ions have been exploited for their circularly polarized luminescence properties for decades[18-20] and that continues with many recent studies.[21-25]

Circularly polarized luminescence (CPL) is the differential emission of left vs right circularly polarized light. The observables in CPL spectroscopy are the difference in emission intensity of left vs right circularly polarized light (I_L-I_R) and sum of the emission intensity of left vs right circularly polarized light ($I_L + I_R$), which is the total luminescence. To compare across systems with different overall emission efficiencies, it is common to use the emission dissymmetry factor, $g_{em}(\lambda)$, shown in Equation 1.

$$g_{em}(\lambda) = \frac{2(I_L(\lambda) - I_R(\lambda))}{(I_L(\lambda) + I_R(\lambda))}, \quad (1)$$

where $I_L(\lambda)$ and $I_R(\lambda)$ are the intensity of left- and right-circularly polarized light at wavelength, λ, respectively. The value of $g_{em}(\lambda)$ can vary between +2 and −2 giving information about both the sign and magnitude of the polarization of light. Chiral lanthanide complexes typically have larger $|g_{em}|$ than chiral transition metal or organic molecules.[18,19] In fact, a chiral europium complex

 © 2019 Wiley Periodicals, Inc.

demonstrates an unusually large g_{em} = +1.38, with ~80% of the emission as left circularly polarized.[26]

The reason that luminescent lanthanides show large CPL comes from the properties of the 4f-4f transitions. The emission dissymmetry factor between two states (1 → 2) is represented by Riehl and Richardson:[20]

$$g_{em} = \frac{4R_{12}}{|D_{12}|}, \quad (2)$$

where R_{12} is the rotatory strength and D_{12} is the dipole strength of the transition. The dipole strength and rotatory strengths are represented by the following:

$$D_{12} = |\langle 1|\hat{\mu}|2\rangle|^2 + |\langle 1|\hat{m}|2\rangle|^2 = |\mu_{12}|^2 + |m_{12}|^2, \quad (3)$$

$$R_{12} = |m_{12}|\cdot|\mu_{12}|\cos\tau_{12}, \quad (4)$$

where μ_{12} and m_{12} are the electric and magnetic dipole transition moment vectors, and τ_{12} is the angle between the vectors. Since the 4f-4f transitions are LaPorte forbidden, they acquire electric dipole transition strength through both static and dynamic coupling mechanisms.[18,27] The static coupling mechanism involves interconfigurational mixing of opposite parity and 4f electron states of the metal through interaction with the ligand field.[27] Therefore, this mechanism depends on the type and arrangement of the ligands about the metal ion. The dynamic coupling mechanism involves coupling a metal-centered 4f-4f electric multipole (eg, quadropole) transition with ligand-centered electric dipole moment transitions (eg, $\pi \rightarrow \pi^*$ transitions).[18,27] Since 4f-4f transitions are magnetic dipole allowed (as long as $\Delta J = 0,\pm1$), the electric dipole transition mechanisms do not always dominate and can lead to large rotatory strengths compared with the dipole strength, resulting in a large g_{em} (Equation 2).

The $^5D_0 \rightarrow {}^7F_1$ transition within the $4f^6$ configuration of Eu^{3+} is an example of a magnetic dipole allowed transition that typically leads to large emission dissymmetry factors, g_{em}. In fact, this is the transition that leads to the unusually large g_{em} = +1.38 in tetrakis((+)-3-heptafluorobutylyrylcamphorato) europium (III).[26] The large g_{em} and small number of Stark levels, leading to simpler to interpret CPL spectra structure, are key factors contributing to the large number of CPL studies involving chiral europium complexes (most with $|g_{em}| > 0.1$).[4,21,22,24,25,28,29] While Eu^{3+} has been widely exploited for CPL applications, there are very few studies involving the CPL of Sm^{3+} complexes.[30-36] This is somewhat surprising given the fact that there are two magnetic-dipole allowed emissive transitions, $^4G_{5/2} \rightarrow {}^6H_{5/2}$ and $^4G_{5/2} \rightarrow {}^6H_{7/2}$, within the $4f^5$ configuration of Sm^{3+}. Additionally, tetrakis((+)-3-heptafluorobutylyrylcamphorato) samarium (III) shows $|g_{em}|$ = 1.15, among the highest measured of all lanthanide complexes, for transitions in both $^4G_{5/2} \rightarrow {}^6H_{5/2}$ and $^4G_{5/2} \rightarrow {}^6H_{7/2}$.[30]

One of the objectives of this study is to further demonstrate that chiral luminescent samarium complexes can give chiroptical properties worth exploiting in chiral luminescence applications (eg, optical displays or biomolecular probes). In order to achieve this objective, lanthanide complexes are prepared with chiral ligands, and the emission dissymmetry factors, g_{em}, are measured. Because direct excitation of 4f-4f transitions is weak, the ligand should be both chiral and act as a sensitizer for the lanthanide emission.[19,37] The ligands with axial chirality used in this study, (*R*)- and (*S*)-2,2'-bis(diphenylphosphoryl)-1,1′-binaphthyl (BINAPO), are shown in Figure 1. The (*R*/*S*)-BINAPO ligands are easy to synthesize[29] and have $\pi \rightarrow \pi^*$ transitions that can sensitize lanthanide luminescence. A chiroptical spectroscopic study of (*R*/*S*)-BINAPO in solid state demonstrates that the emission shows an observable CPL spectrum[10] at 355 nm. Harada et al[29,38] have studied the CPL of BINAPO complexes with europium that demonstrated that BINAPO can act as a sensitizer and generate chirality in the emission. However, the largest g_{em}'s came from complexes with additional chiral ligands, and the study did not extend to samarium complexes. In this study, chiral complexes are formed by mixing Eu $(OTf)_3$ and Sm $(OTf)_3$ (where OTf = trifluoromethane sulfonate) with the (*R*/*S*)-BINAPO ligands. Because the $^5D_0 \rightarrow {}^7F_{0-2}$ luminescence spectrum of europium is easier to interpret, the ratio of the BINAPO:Ln $(OTf)_3$ (where Ln = Eu or Sm) emitting complex is determined by titrating BINAPO with a constant concentration of Eu $(OTf)_3$ to be 2:1. The CPL of the resulting samarium and europium complexes are presented and characterized. Ab initio quantum chemical calculations offer a prediction of the structure of the samarium and europium BINAPO complexes that is consistent with experimental titration and CPL spectroscopic data.

2 | MATERIALS AND METHODS

(*R*/*S*)-2,2'-bis(diphenylphosphino)-1,1′-binaphthyl ((*R*/*S*)-BINAP) was purchased from Strem chemicals and used without further purification. Europium Tris (trifluoromethane

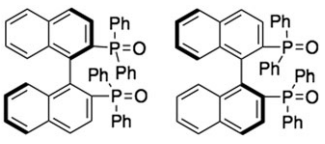

FIGURE 1 Structures of chiral ligands, (*R*)- and (*S*)-BINAPO

sulfonate) (Eu $(OTf)_3$), samarium Tris (trifluoromethane sulfonate) (Sm $(OTf)_3$), and lutetium Tris (trifluoromethane sulfonate) (Lu $(OTf)_3$) were purchased from Sigma-Aldrich and used without further purification. Deuterated solvents, chloroform and methanol, were purchased from Cambridge Isotopes Laboratories.

2.1 | Preparation of (*R*/*S*)-2,2'-bis(diphenylphosphoryl)-1,1′-binaphthyl (*R*/*S*-BINAPO)

(*R*/*S*)-BINAPO was prepared using a literature procedure.[29] (*R*/*S*)-BINAPO was dissolved in dichloromethane, stirred for ~1 hour at 0°C, and then an excess of 30% hydrogen peroxide solution was added dropwise. The resulting solution was stirred under nitrogen for ~16 hours and quenched with water. The solution was extracted with dichloromethane (three times), and the dichloromethane phase was dried with magnesium sulfate. The resulting solution was filtered, the solvent was removed with a rotary evaporator, and recrystallization in methanol/water gave white powder/crystals. *S*-BINAPO mp 258°C, ^{1}H NMR ($CDCl_3$, 400 MHz) δ 7.85-7.80 (m, 4H), 7.70-7.65 (q, 4H), 7.45-7.30 (m, 12H), 7.25-7.20 (m, 8H), 6.80 (d, 4H). FTIR (ATR) 1433 (m), 1305 (w), 1199 (s, P=O), 1116 (s), 1100 (m), 870 (w, aromatic), 814 (m, aromatic), 746 (s, aromatic), 722 (s, aromatic), 695 (s, aromatic) cm^{-1}.

2.2 | Preparation of LN $(OTf)_3$((*R*/*S*)-BINAPO)$_X$ (where LN = EU, LU, OR SM) samples

Solutions were created by combining 0.010 M Eu $(OTf)_3$, 0.010 M Lu $(OTf)_3$ 0.010, or 0.0025 M Sm $(OTf)_3$ with (*R*)- or (*S*)-BINAPO in methanol to achieve 1:2 stoichiometric ratio of Ln:BINAPO. These solutions were used for spectroscopic analysis. Ethyl acetate was added to the solution to precipitate the Eu $(BINAPO)_2(OTf)_3$ complex as a white powder for FTIR analysis. Solutions made from dissolving precipitated Eu $(BINAPO)_2(OTf)_3$ in methanol were also used for spectroscopic analysis. Lu((*S*)-BINAPO)$_2$(OTf)$_3$ ^{1}H-NMR ($CDCl_3$, 400 MHz) δ 7.70-6.60 (m, aromatic). Eu((*R*)-BINAPO)$_2$(OTf)$_3$ FTIR (ATR) 3500-3000 (br), 1589 (s), 1438 (s), 1272 (s, S=O), 1223 (w, C-F), 1150-1130 (br, P=O), 1115 (s), 1084 (m), 1030 (w, S=O), 875 (w, aromatic), 820 (m, aromatic), 746 (s, aromatic), 722 (s, aromatic), 702 (s, aromatic) cm^{-1}. Sm((*R*)-BINAPO)$_2$(OTf)$_3$ FTIR (ATR) 3400 (br), 1660 (m), 1636 (m), 1438 (w), 1241 (br, S=O, C-F), 1185 (s, P=O), 1117 (m), 1029 (s, S=), 875 (w, aromatic), 816 (w, aromatic), 749 (w, aromatic), 725 (m, aromatic), 703 (s, aromatic) cm^{-1}.

2.3 | Titration analysis

The complexation titration samples were created by adding 0.000628-0.0075 M BINAPO to 0.0025 M Eu $(OTf)_3$ in methanol. A total of seven samples were created with BINAPO:Eu ratio of 0.25:1-3:1. The emission spectrum of each solution was measured at an excitation wavelength (355 nm) corresponding to BINAPO excitation. The emission intensities were determined by measuring the area under the $^5D_0 \rightarrow {}^7F_2$ peak (605-625 nm).

2.4 | Spectroscopic analysis

Emission and excitation spectra of the samples were measured using a Perkin-Elmer LS-55 Luminescence Spectrometer. Circularly polarized luminescence spectra and luminescence lifetimes were recorded on instrumentation assembled in our lab and described previously.[39] ^{1}H-NMR spectra for BINAPO were recorded on a Bruker 400 MHz NMR. IR spectra for BINAPO and Eu $(BINAPO)_2(OTf)_3$ were recorded on a Thermo Scientific Smart OMNI-Transmission Nicolet iS10 with the Smart iTR accessory.

2.5 | Computational methods

Initial components of the Sm $(BINAPO)_2(OTf)_3$ complex were built and assembled[40] using Avogadro, version 1.2. All electronic structure calculations were performed using GAMESS version[41] April 20, 2017, along with companion program MacMolPlt,[42] version 7.7. The images presented were produced using VMD,[43] version 1.9.2. Without an available experimental three-dimensional structure for the complex, it was important to build and refine a structure that matched experimental stoichiometry. In order to exhibit CPL, the structure of the samarium complex must belong to a chiral point group with only proper rotations. Therefore, these requirements were imposed and monitored on the stepwise building and refinement process. An initial conformation for BINAPO was built in the *S* configuration with the two phosphoryl groups roughly eclipsing each other. After initial optimization using the semiempirical PM3 method,[44,45] the structure was reoriented so as to insure D_2 point group symmetry. Subsequent ab initio RHF optimization was done imposing D_2 symmetry, using the all electron 6-31G basis set,[46-48] supplemented with appropriate polarization functions (d-type Gaussians on C, O, P, and p-type Gaussians on H) on all atoms.[49]

In the next step, a Sm((*S*)-BINAPO)$_2$ complex was constructed by placing the Sm (III) ion at the coordinate origin, and two copies of the refined *S*-BINAPO structure positioned symmetrically along the X-axis. This was done so as to have the four phosphoryl oxygens, of two (*S*)-BINAPO groups, symmetrically positioned approximately 3.0 Angstroms from the Sm (III) ion, in a square planer arrangement. The initial complex possessed D_2 symmetry that was imposed during the subsequent *ab initio* UHF optimization. Again, the 6-31G** basis set was used for all *S*-BINAPO atoms. The lanthanide ions (Sm^{3+} and Eu^{3+}) were treated using the SBKJC effective core potentials and associated valence basis set.[50]

Starting from the optimized Sm((*S*)-BINAPO)$_2$ structure, it was determined that an initial arrangement possessing C_2 symmetry was possible if two OTf^- ligands were symmetrically placed along the Y-axis. The OTf^- ligands were initially arranged with the three sulfonate oxygens complexing the Sm (III) at approximately 3.0 Angstroms distance. Although this arrangement gives the complex the unusual coordination number of 10, it was expected that optimization would likely reduce this. Optimization of the complex used the same basis set treatment for the Sm(*S*-BINAPO)$_2$ portion as previously described. However, each OTf^- was treated using the 6-31G* basis set, along with the addition of a diffuse function on each of the O and S atoms of the sulfonate groups.[51] Ab initio UHF optimization proceeded to convergence with C_2 symmetry imposed to produce the Sm(*S*-BINAPO)$_2$(OTf)$_2$ complex with an overall +1 charge. Finally, an equivalent Eu((*S*)-BINAPO)$_2$(OTF)$_2^+$ complex was produced by replacing the Sm (III) atom with Eu (III) in the final optimized Sm (III) structure. The ab initio UHF optimization was reinitialized and proceeded to convergence.

3 | RESULTS AND DISCUSSION

3.1 | Spectroscopic results

Samples were prepared by mixing molar ratios of the (*R*/*S*)-BINAPO with Eu (OTf)$_3$ (or Sm (OTf)$_3$) in methanol and allowing the mixture to establish an equilibrium. ATR-FTIR spectra (shown in Figure S1) of (*R*)-BINAPO vs Eu((*R*)-BINAPO)$_2$(OTf)$_3$ and Sm((*R*)-BINAPO)$_2$(OTf)$_3$ show almost identical BINAPO peak locations for all of the peaks except for those assigned to the P=O stretch. In (*R*)-BINAPO, the peak at 1200 cm^{-1} is assigned to the P=O stretch,[29] but in both Eu((*R*)-BINAPO)$_2$(OTf)$_3$ and Sm((*R*)-BINAPO)$_2$(OTf)$_3$, this peak shifts to between 1185 and 1150 cm^{-1} indicating that the P=O bonds are weakened by coordination to the Eu^{3+} and Sm^{3+}.

The emission spectra for the $^5D_0 \rightarrow {}^7F_{0-3}$ transitions of Eu^{3+} in Eu((*R*)-BINAPO)$_2$(OTf)$_3$ and $^4G_{5/2} \rightarrow {}^6H_{5/2-9/2}$ transitions of Sm^{3+} in Sm((*R*)-BINAPO)$_2$(OTf)$_3$ are shown in Figure 2. The excitation wavelength of 355 nm overlaps with a BINAPO electronic transition,[10] which shows that BINAPO sensitizes both Eu^{3+} and Sm^{3+} luminescence. Because these are room temperature solution phase measurements, the individual Stark level to Stark level transitions are not resolved enough to determine the site symmetry at the Eu^{3+} or Sm^{3+}, but the spectra in Figure 2 show 4f-4f transition locations that are typical for Eu^{3+} and Sm^{3+}. Samples created by dissolving the recrystallized Eu((*R*)-BINAPO)$_2$(OTf)$_3$ in methanol gave identical emission spectra as shown in Figure 2.

The luminescence lifetime (trace shown in Figure S1) for the $^5D_0$ state of Eu((*R*)-BINAPO)$_2$(OTf)$_3$ was monexponential with a lifetime in methanol of 993 μs and 1.157 ms in deuterated methanol. Unfortunately, the luminescence lifetime of the $^4G_{5/2}$ state of Sm((*R*)-BINAPO)$_2$(OTf)$_3$ is too short (<100 μs) to reliably measure with our instrumentation. There is an accepted empirical formula (ie, Horrocks equation) for determining the number of coordinated waters to Eu^{3+} by comparing $^5D_0$ luminescence lifetimes in H_2O vs D_2O.[52] Assuming that the O—H oscillator in methanol is as effective at quenching as O—H in water, the equation can be modified (see Figure S1) to estimate the number of coordinating methanol molecules using lifetimes in methanol and deuterated methanol.[53] Based on the Horrocks equation, these lifetimes predict that there are 0.3 ± 0.5 methanol molecules coordinating to Eu^{3+}, essentially no solvent coordination.

The luminescence lifetime, 993 μs, of Eu((*R*)-BINAPO)$_2$(OTf)$_3$ can be used determine the intrinsic quantum yield of the Eu^{3+} according to the following:

$$Q = \frac{\tau_{obs}}{\tau_{rad}}, \tag{5}$$

where τ_{obs} is the experimental lifetime, and τ_{rad} is the radiative lifetime. This can be estimated by Bünzli[37]:

$$\frac{1}{\tau_{rad}} = A_{md} n^3 \left(\frac{I_{tot}}{I_{md}}\right), \tag{6}$$

where A_{md} = 14.65 s^{-1}, n = 1.329 (refractive index of methanol), I_{tot} is the integrated intensity for $^5D_0 \rightarrow {}^7F_{0-6}$ transitions, and I_{md} is the integrated intensity for the $^5D_0 \rightarrow {}^7F_1$ transition. This leads to a τ_{rad} = 4.79 ms. Inserting these values into Equation 5 gives an intrinsic quantum yield of 0.17.

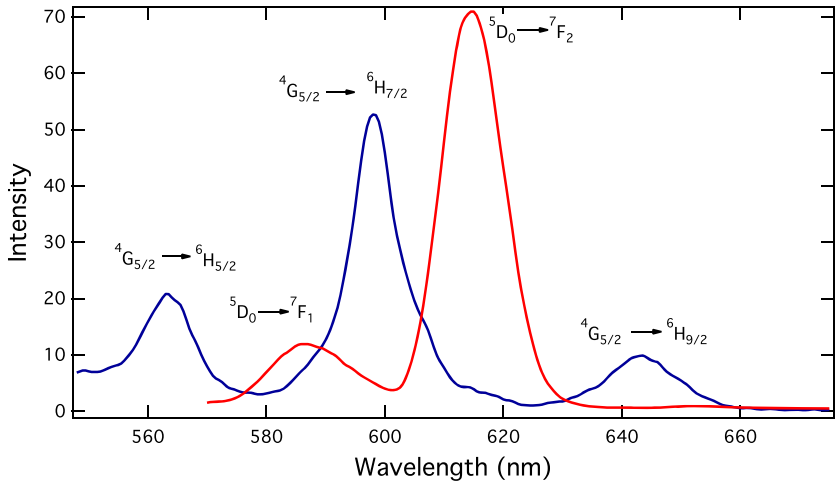

FIGURE 2 Emission spectra for the $^5D_0 \rightarrow {}^7F_{0-3}$ transitions of 0.010 M Eu((*R*)-BINAPO)$_2$(OTf)$_3$ (red) and the $^4G_{5/2} \rightarrow {}^6H_{5/2-9/2}$ transitions of 0.010 M Sm((*R*)-BINAPO)$_2$(OTf)$_3$ (blue) in methanol. The excitation wavelength is 355 nm

4 | COMPLEXATION TITRATION

The titration of Eu (OTf)$_3$ with increasing concentrations of BINAPO resulted in an increase in emission intensity from the 4f-4f transitions of Eu^{3+}. Figure 3 shows the emission intensity vs BINAPO concentration for 0.0025M Eu (OTf)$_3$, where the BINAPO concentration ranges from 0.000628 to 0.0075M (BINAPO:Eu ratio of 0.25:1-3:1). Because the excitation wavelength excites only Eu^{3+} coordinated by BINAPO ligand(s), the emission intensity is a direct measure of the concentration of the Eu (BINAPO)$_x$ (OTf)$_y$ complex. While the overall intensity increases with increased BINAPO concentration, the peak locations and relative intensities of the peaks within a spectrum were unchanged. Because the location and relative intensities of 4f-4f transitions are sensitive to the coordination environment of the Eu^{3+}, the titration data is consistent with a single major Eu-BINAPO emitting species. This is further evidenced by the fact that the observed CPL spectra (Figure 5 and Figure S6) also does not change as the Eu (OTf)$_3$:BINAPO ratio changes. This indicates that the equilibrium in methanol is a single-step complexation equilibrium.

$$\mathrm{Eu(OTf)_3 + xBINAPO} \rightleftharpoons \mathrm{Eu(BINAPO)_x(OTf)_y} \tag{7}$$

with equilibrium constant,

$$\beta = \frac{\left[Eu(BINAPO)_x(OTf)_y\right]}{\left[Eu(OTf)_3\right]\left[BINAPO\right]^x}. \tag{8}$$

The data in Figure 3 fit to a modified Hill equation shown in Equation 9:

$$I = I_0 + \frac{I_{max} - I_0}{1 + \left(\frac{[BINAPO]_{1/2}}{[BINAPO]_0}\right)^n}, \tag{9}$$

where I is emission intensity, I_0 is the emission intensity with no BINAPO added, I_{max} is the maximum emission intensity, $[BINAPO]_{1/2}$ is the $[BINAPO]_0$ at 50% of the

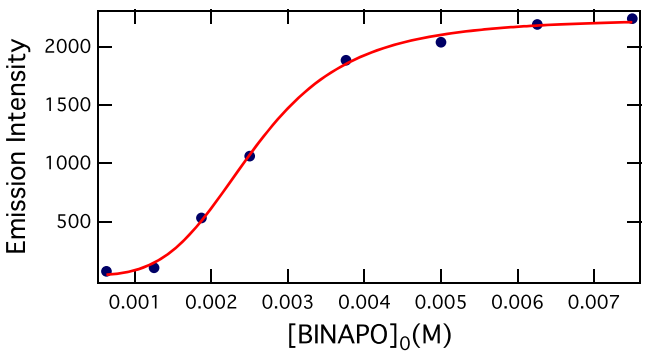

FIGURE 3 Integrated emission intensity of the $^5D_0 \rightarrow {}^7F_2$ region of Eu((*R*)-BINAPO)$_2$(OTf)$_3$ vs [BINAPO] added. The red line is a fit of the Hill equation to the data. The excitation wavelength is 355 nm

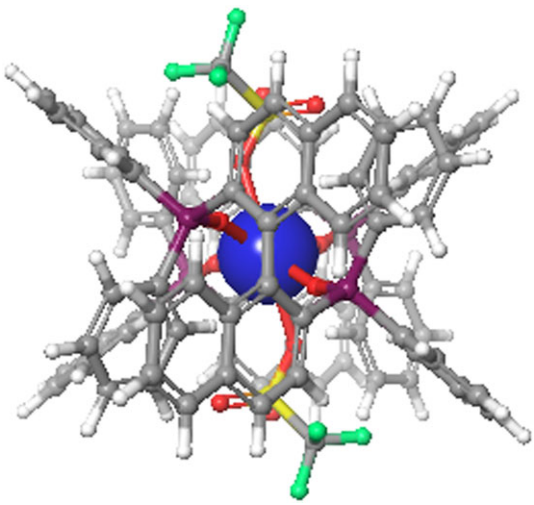

FIGURE 4 Calculated structure of [Sm((*S*)-BINAPO)$_2$(OTf)$_2$]$^+$ shown along the C_2 axis

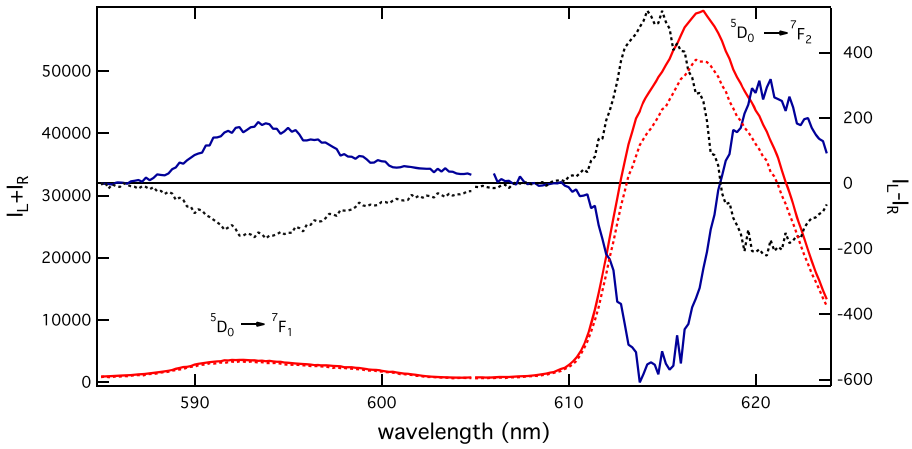

FIGURE 5 Total luminescence (red) and CPL spectra (blue) of the $^5D_0 \rightarrow {}^7F_{1,2}$ transitions for 0.010 M Eu((*R*)- (solid lines) vs (*S*)-BINAPO)$_2$(OTf)$_3$ (dotted lines). The excitation wavelength is 355 nm

maximum emission intensity, or the dissociation constant, and n is the Hill coefficient. The fit of the titration data to Equation 6 gave $[BINAPO]_{1/2} = 0.00257 \pm 0.00006$ M, and $n = 4.0 \pm 0.4$. The Hill coefficient, $n > 1$, indicates that there are multiple BINAPO ligands binding ($x > 1$ in Equation 5) to the europium, and that the binding is cooperative.[54] Assuming that $[BINAPO]_{1/2}$ (half the maximum emission intensity) represents the complexation of half of $[Eu]_0$, the ratio of Eu: BINAPO is 1:2 (0.00125:0.00257 M) and therefore $x = 2$. The equilibrium constant, β, can be estimated by assuming that $K_d = ([BINAPO]_{1/2})^2$, where K_d is the dissociation constant, and $\beta = 1/K_d$. Using the values from a fit of the titration data in Figure 3, $\log\beta = 5.20$ for the equilibrium shown in Equation 7 in methanol at room temperature (293 K).

The titration and spectroscopic data suggests that the emissive species in methanol is Eu (BINAPO)$_2$(OTf)$_y$, and the methanol vs deuterated methanol lifetime shows that there are no methanol molecules coordinating Eu^{3+}. Since the small ionic size difference between Sm^{3+} and Eu^{3+} does not typically result in large variations in chemical behavior, it can be assumed that the structure at the metal ion is very similar. Therefore, in this study, it is also assumed that Sm (BINAPO)$_2$(OTf)$_y$ is the primary emitting species in the samarium samples. The experimental data shows four of the coordination sites to the Sm^{3+} or Eu^{3+} but cannot show how many (or if) OTf^- ligands are also coordinated to the metal.

5 | CALCULATIONS

Calculations are used to predict the coordination structure, including the number and possible orientation of OTf^- ligands. Figure 4 shows the optimized structure calculated, which is [Sm((*S*)-BINAPO)$_2$(OTf)$_2$]$^+$. As shown in Figure 4, the two BINAPO ligands are bulky enough to optimize to a six-coordinate Sm^{3+} structure with two triflate oxygens (one each) coordinating along with the four phosphoryl oxygens. Attempts to construct structure with multidentate OTf^- ligands converged to monodentate. This six-coordinate Sm^{3+} or Eu^{3+} is unusual but not without precedent.[55-58] The symmetry of the [Sm((S)-BINAPO)$_2$(OTf)$_2$]$^+$ (Figure 4), and site symmetry at the Sm (or Eu) is C_2, a chiral point group The chiral arrangement of the BINAPO and OTf^- ligands around the metal center satisfies the requirement for a

TABLE 1 Emission dissymmetry factors for europium BINAPO complexes

$^5D_0 \rightarrow {}^7F_1$	Eu((*R*)-BINAPO)$_2$(OTf)$_3$[a]	Eu((*S*)-BINAPO)$_2$ (OTf)$_3$	Eu((*R*)-BINAPO)(D-facam)$_3$	Eu((*R*)-BINAPO)(hfa)$_3$
g_{em}(593)	0.120(8)	−0.110(8)	−0.44 (594 nm)[b]	0.03[b]
$^5D_0 \rightarrow {}^7F_2$				
g_{em}(614)	−0.026(1)	0.025(1)	0.029 (613 nm)[b]	0.003[b]
g_{em}(620)	0.014(1)	−0.012(1)		

[a]g_{em}'s are the same for 1:1, 1:2, and 1:3 Eu (OTf)$_3$:*R*- and *S*-BINAPO samples. Uncertainties are in parentheses.

[b]g_{em}'s are from Harada et al.[28]

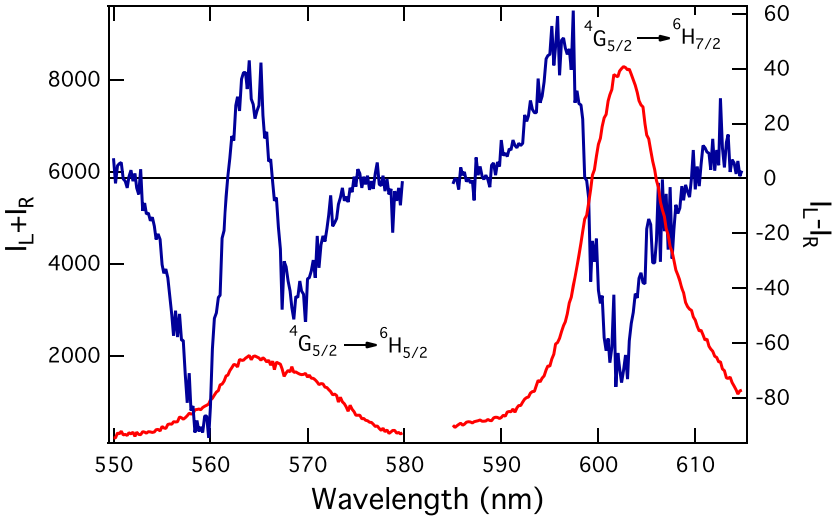

FIGURE 6 Total luminescence and CPL spectra of the $^4G_{5/2} \rightarrow {}^6H_{5/2}$, $^6H_{7/2}$ transition for 0.0025M Sm((*R*)-BINAPO)$_2$(OTf)$_3$. The excitation wavelength is 355 nm

static coupling mechanism leading to dipole and rotatory strengths for magnetic-dipole allowed CPL transitions[18,27] in Eu^{3+} and Sm^{3+}. Because the BINAPO ligands have $\pi \rightarrow \pi^*$ transitions, the dipole and rotatory strengths could also derive from the dynamic coupling mechanism between the Eu^{3+} or Sm^{3+} electric quadrupole (or larger multipole) moment and ligand $\pi \rightarrow \pi^*$ transitions.[18,27] Therefore, the structure predicted in Figure 4 is consistent with CPL spectra and emission dissymmetry factors, g_{em}, derived from a combination of the static and dynamic coupling mechanisms.

6 | CPL SPECTROSCOPY

The CPL and total luminescence spectra of the $^5D_0 \rightarrow {}^7F_{1,2}$ transitions for Eu((*R*)- vs (*S*)-BINAPO)$_2$(OTf)$_3$ are shown in Figure 5. The locations of the $^5D_0 \rightarrow {}^7F_1$ and$^5D_0 \rightarrow {}^7F_2$ total luminescence transitions are identical for (R)- vs. (S)-BINAPO. However, the CPL spectra of the $^5D_0 \rightarrow {}^7F_1$ transition (Figure 5) shows one broad peak centered at 593 nm that corresponds to the maximum of the peak in the total luminescence. These peaks are opposite in sign and nearly equal in magnitude for (*R*)- (positive CPL) vs (*S*)-BINAPO (negative CPL). The CPL spectra of the $^5D_0 \rightarrow {}^7F_2$ transition (Figure 5) show two peaks of opposite sign located at 614 and 620 nm. Neither of these peaks matches the location of the maximum of the $^5D_0 \rightarrow {}^7F_2$ transition in the total luminescence, but there is evidence of two shoulders that match the locations of the two CPL peaks. The CPL peaks of the $^5D_0 \rightarrow {}^7F_2$ transition are also opposite in sign and nearly equal in magnitude for (*R*)- vs (*S*)-BINAPO.

Table 1 shows that the $g_{em}(\lambda)$ determined for Eu((*R*)- vs (*S*)-BINAPO)$_2$(OTf)$_3$ complexes are opposite sign and equal in magnitude. The magnitude of $g_{em}(\lambda)$ for the $^5D_0 \rightarrow {}^7F_1$ transitions are five to eight times larger than the $g_{em}(\lambda)$ for $^5D_0 \rightarrow {}^7F_2$ transitions. For comparison purposes, Table 1 includes g_{em} values observed by Harada et al[29,38] for Eu((*R*)-BINAPO)(D-facam)$_3$ and Eu((*R*)-BINAPO)(hfa)$_3$ (where facam = 3-trifluoroacetyl-d-camphor and hfa = 1,1,1,5,5,5-hexafluoropentane-2,4-dione). Eu((*R*)-BINAPO)(D-facam)$_3$ has the largest magnitude g_{em} shown in the table, but the magnitude and sign of g_{em} are primarily a result of coordination by the D-facam ligands.[29] Eu(*R*-BINAPO)(hfa)$_3$ derives its

TABLE 2 Emission dissymmetry factors for samarium BINAPO complexes

$^4G_{5/2} \rightarrow {}^6H_{5/2}$	Sm((*R*)-BINAPO)$_2$(OTf)$_3$[a]	Sm((*S*)-BINAPO)$_2$(OTf)$_3$
$g_{em}(559)$	−0.224(9)	0.272(9)
$g_{em}(564)$	0.036(6)	−0.062(6)
$g_{em}(569)$	−0.054(6)	0.064(6)
$^4G_{5/2} \rightarrow {}^6H_{7/2}$		
$g_{em}(595)$	0.050(6)	−0.068(6)
$g_{em}(602)$	−0.016(2)	0.017(2)

[a]Uncertainties are shown in parentheses.

chirality and CPL (g_{em}) from the R-BINAPO ligand similar to Eu(*R*-BINAPO)$_2$(OTf)$_3$, but the number of BINAPO ligands coordinated to the europium ion is different. While the signs of the g_{em} for Eu(*R*-BINAPO)(hfa)$_3$ and Eu(*R*-BINAPO)$_2$(OTf)$_3$ are the same, Eu(*R*-BINAPO)$_2$(OTf)$_3$ has a much larger magnitude.

The CPL and total luminescence spectrum of the $^4G_{5/2} \rightarrow {}^6H_{5/2}$, $^6H_{7/2}$ transitions of Sm((*R*)-Binapo)$_2$(OTf)$_3$ is shown in Figure 6. The CPL spectrum of the $^4G_{5/2} \rightarrow {}^6H_{5/2}$ transition shows three distinct transitions (two negative and one positive) at 559, 565, and 569 nm. The peak at 565 nm corresponds to the maximum and the locations of the other two peaks are not as evident in the total luminescence spectrum. If the emission originates from only one Stark level in $^4G_{5/2}$, the CPL spectrum is showing the location of all three energy levels (Kramers doublets) in the $^6H_{5/2}$ multiplet. Since all transitions are symmetry allowed in C_2 symmetry, the spectrum (Figure 6) is consistent with the calculated structure (Figure 4).[59] The CPL spectrum of the $^4G_{5/2} \rightarrow {}^6H_{7/2}$ transition shows two peaks (negative and positive) at 595 and 602 nm. The peak at 602 nm is coincident with the peak maximum in the total luminescence spectrum for the $^4G_{5/2} \rightarrow {}^6H_{7/2}$ transition. The CPL spectrum for Sm((*S*)-BINAPO)$_2$(OTf)$_3$ shows identical peak locations for the total luminescence and CPL but opposite signs for the CPL peaks (Figure S1).

The g_{em} values determined at each of the CPL peak transition are shown in Table 2. All of the $|g_{em}|$ shown in Table 2 are larger in magnitude for the complex with (*S*)- vs (*R*)-BINAPO, but the difference in $|g_{em}|$ at 559, 564, and 595 nm is outside of the uncertainty in the measurement. Unfortunately, the experimental and calculated structural information in this study is not detailed enough to rationalize these differences in rotatory strengths for 4f-4f transitions. However, the average $|g_{em}| = 0.25$ at 559 nm for Sm((*R*/*S*)-BINAPO)$_2$(OTf)$_3$ shown in Table 2 is among the largest dissymmetry factors observed for a Sm^{3+} complex in solution. One of the reasons for the large g_{em} is the small dipole strength of this transition ($|D_{12}|$ in Equation 2), but this transition also has a relatively large rotatory strength as evidenced by the fact that it exhibits the largest CPL intensity in Figure 6. The rest of the transitions in Figure 6, including the most intense luminescence transitions at 564 and 602 nm, have $|g_{em}| \sim 10^{-2}$. The $|g_{em}|$ at 559 nm in Sm((*S*)-BINAPO)$_2$(OTf)$_3$ is more than double the largest g_{em} observed (0.120) for Eu((*R*)- or (*S*)-BINAPO)$_2$(OTf)$_3$ (Table 1). Although there are not very many examples of Sm^{3+} CPL in the literature, BINAPO appears to be the only chiral ligand that induces a larger g_{em} for the magnetic dipole allowed transitions in Sm^{3+} vs Eu^{3+}.

7 | CONCLUSION

This study reports CPL studies of both Eu^{3+} and Sm^{3+} coordinated by chiral ligand, (*R*)- and (*S*)-BINAPO. Titration data show that the coordination complex formed in methanol is 2:1 BINAPO:Ln^{3+}, and lifetime measurements show that solvent (methanol) is not coordinating the metal ions. The resulting Eu((*R*/*S*)-BINAPO)$_2$(OTf)$_3$ and Sm((*R*/*S*)-BINAPO)$_2$(OTf)$_3$ complexes show strong CPL signal with opposite sign for opposite BINAPO enantiomers. The measured $|g_{em}|$ for the $^5D_0 \rightarrow {}^7F_{1,2}$ regions are large but not unusual for chiral Eu^{3+} complexes. However, the measured $|g_{em}|$ for the $^4G_{5/2} \rightarrow {}^6H_{5/2}$ region is among the largest reported for a chiral Sm^{3+} complex in solution. Additionally, (*R*)/(S)-BINAPO is the first chiral ligand system that gives a larger g_{em} for Sm^{3+} vs Eu^{3+}. These promising CPL results for Sm((*R*/*S*)-BINAPO)$_2$(OTf)$_3$ are unlikely to be unique to the BINAPO ligand. The data in this study combined with those of some other recent studies[30,31,35,36] should encourage more exploration of chiral Sm^{3+} complexes for CPL applications.

ACKNOWLEDGEMENTS

The authors would like to acknowledge Matt Goldey for writing the CPL instrument software. The authors would also like to thank the Butler Program for Undergraduate Research for funding to support this work.

ORCID

Todd A. Hopkins https://orcid.org/0000-0001-9943-6047

REFERENCES

1. Urey H, Chellappan KV, Erden E, Surman P. State of the art in stereoscopic and autostereoscopic displays. *Proc IEEE*. 2011;99(4):540-555. https://doi.org/10.1109/JPROC.2010.2098351
2. Bennett CH, DiVincenzo DP. Quantum information and computation. *Nature*. 2000;404(6775):247-255. https://doi.org/10.1038/35005001
3. Jennings L, Waters RS, Pal R, Parker D. Induced europium circularly polarized luminescence monitors reversible drug binding to native A1-acid glycoprotein. *ChemMedChem*. 2017;12(3):271-277. https://doi.org/10.1002/cmdc.201600571
4. Neil ER, Fox MA, Pal R, Parker D. Induced europium CPL for the selective signalling of phosphorylated amino-acids and O-phosphorylated hexapeptides. *Dalton Trans*. 2016;45(20):8355-8366. https://doi.org/10.1039/C6DT01212D
5. Ray C, Sánchez-Carnerero EM, Moreno F, et al. Bis (HaloBODIPYs) with labile helicity: valuable simple organic molecules that enable circularly polarized luminescence. *Chem*

Eur J. 2016;22(26):8805-8808. https://doi.org/10.1002/chem.201601463

6. Sánchez-Carnerero EM, Agarrabeitia AR, Moreno F, et al. Circularly polarized luminescence from simple organic molecules. *Chem Eur J*. 2015;21(39):13488-13500. https://doi.org/10.1002/chem.201501178
7. Saleh N, Moore B, Srebro M, et al. Acid/base-triggered switching of circularly polarized luminescence and electronic circular dichroism in organic and organometallic helicenes. *Chem Eur J*. 2015;21(4):1673-1681. https://doi.org/10.1002/chem.201405176
8. Alnoman RB, Rihn S, O'Connor DC, et al. Circularly polarized luminescence from helically chiral *N*,*N*,*O*,*O*-boron-chelated dipyrromethenes. *Chem Eur J*. 2016;22(1):93-96. https://doi.org/10.1002/chem.201504484
9. Feuillastre S, Pauton M, Gao L, et al. Design and synthesis of new circularly polarized thermally activated delayed fluorescence emitters. *J Am Chem Soc*. 2016;138(12):3990-3993. https://doi.org/10.1021/jacs.6b00850
10. Kono Y, Nakabayashi K, Kitamura S, Kuroda R, Fujiki M, Imai Y. A comparison of circularly polarised luminescent BINAP and BINAPO as chiral binaphthyl luminophores. *Tetrahedron*. 2015;71(23):3985-3989. https://doi.org/10.1016/j.tet.2015.04.048
11. Delgado IH, Pascal S, Wallabregue A, et al. Functionalized cationic [4] helicenes with unique tuning of absorption, fluorescence and chiroptical properties up to the far-red range. *Chem Sci*. 2016;7(7):4685-4693. https://doi.org/10.1039/C6SC00614K
12. Sannicolò F, Mussini PR, Benincori T, et al. Inherently chiral macrocyclic oligothiophenes: easily accessible electrosensitive cavities with outstanding enantioselection performances. *Chem Eur J*. 2014;20(47):15298-15302. https://doi.org/10.1002/chem.201404331
13. Pascal S, Besnard C, Zinna F, et al. Zwitterionic [4] helicene: a water-soluble and reversible PH-triggered ECD/CPL chiroptical switch in the UV and red spectral regions. *Org Biomol Chem*. 2016;14(20):4590-4594. https://doi.org/10.1039/C6OB00752J
14. Zhao B, Pan K, Deng J. Intense circularly polarized luminescence contributed by helical chirality of monosubstituted polyacetylenes. *Macromolecules*. 2018;51(18):7104-7111. https://doi.org/10.1021/acs.macromol.8b01545
15. Coe BJ, Helliwell M, Sánchez S, Peers MK, Scrutton NS. Water-soluble Ir (III) complexes of deprotonated N-methylbipyridinium ligands: fluorine-free blue emitters. *Dalton Trans*. 2015;44(35):15420-15423. https://doi.org/10.1039/C5DT02591E
16. Zhang X-P, Chang VY, Liu J, et al. Potential switchable circularly polarized luminescence from chiral cyclometalated platinum (II) complexes. *Inorg Chem*. 2014;54(1):143-152. https://doi.org/10.1021/ic5019136
17. Saleh N, Srebro M, Reynaldo T, et al. Enantio-enriched CPL-active helicene–bipyridine–rhenium complexes. *Chem Commun*. 2015. https://doi.org/10.1039/C5CC00453E;51(18):3754-3757
18. Zinna F, Di Bari L. Lanthanide circularly polarized luminescence: bases and applications. *Chirality*. 2015;27(1):1-13. https://doi.org/10.1002/chir.22382
19. Carr R, Evans NH, Parker D. Lanthanide complexes as chiral probes exploiting circularly polarized luminescence. *Chem Soc Rev*. 2012;41(23):7673-7686. https://doi.org/10.1039/c2cs35242g
20. Riehl JP, Richardson FS. Circularly polarized luminescence spectroscopy. *Chem Rev*. 1986;86(1):1-16. https://doi.org/10.1021/cr00071a001
21. Leonzio M, Melchior A, Faura G, et al. Strongly circularly polarized emission from water-soluble Eu (III)- and Tb (III)-based complexes: a structural and spectroscopic study. *Inorg Chem*. 2017;56(8):4413-4421. https://doi.org/10.1021/acs.inorgchem.7b00430
22. Kono Y, Hara N, Shizuma M, Fujiki M, Imai Y. Complexes of Eu (III)(Hfa) 3 with a planar chiral P (III) ligand (phanephos): solvent-sensitive sign inversion of circularly polarised luminescence. *Dalton Trans*. 2017;46(16):5170-5174. https://doi.org/10.1039/C7DT00741H
23. Casanovas B, Zinna F, Bari LD, Fallah MSE, Font-Bardía M, Vicente R. Circularly polarized luminescence on dinuclear Tb (III) and Eu (III) complexes with (*S*-) and (*R*-) 2-phenylpropionate. *Dalton Trans*. 2017;46(19):6349-6357. https://doi.org/10.1039/C6DT04686J
24. Zercher B, Hopkins TA. Induction of circularly polarized luminescence from europium by amino acid based ionic liquids. *Inorg Chem*. 2016;55(21):10899-10906. https://doi.org/10.1021/acs.inorgchem.6b01343
25. Dai L, Lo W-S, Coates ID, Pal R, Law G-L. New class of bright and highly stable chiral cyclen europium complexes for circularly polarized luminescence applications. *Inorg Chem*. 2016;55(17):9065-9070. https://doi.org/10.1021/acs.inorgchem.6b01546
26. Lunkley JL, Shirotani D, Yamanari K, Kaizaki S, Muller G. Extraordinary circularly polarized luminescence activity exhibited by cesium tetrakis(3-heptafluoro-butylryl-(+)-camphorato) Eu (III) complexes in EtOH and $CHCl_3$ solutions. *J Am Chem Soc*. 2008;130(42):13814-13815. https://doi.org/10.1021/ja805681w
27. Richardson FS, Faulkner TR. Optical activity of the f–f transitions in trigonal dihedral (D3) lanthanide (III) complexes. I. Theory. *J Chem Phys*. 1982;76(4):1595-1606. https://doi.org/10.1063/1.443197
28. Uchida T, Nozaki K, Iwamura M. Chiral sensing of various amino acids using induced circularly polarized luminescence from europium (III) complexes of phenanthroline dicarboxylic acid derivatives. *Chem – Asian J*. 2016;11(17):2415-2422. https://doi.org/10.1002/asia.201600798
29. Harada T, Nakano Y, Fujiki M, Naito M, Kawai T, Hasegawa Y. Circularly polarized luminescence of Eu (III) complexes with point- and axis-chiral ligands dependent on coordination structures. *Inorg Chem*. 2009;48(23):11242-11250. https://doi.org/10.1021/ic901663w
30. Lunkley JL, Shirotani D, Yamanari K, Kaizaki S, Muller G. Chiroptical spectra of a series of tetrakis((+)-3-heptafluorobutylyrylcamphorato)lanthanide (III) with an encapsulated alkali metal ion: circularly polarized luminescence and absolute chiral structures for the Eu (III) and Sm (III) complexes. *Inorg Chem*. 2011;50(24):12724-12732. https://doi.org/10.1021/ic201851r

31. Petoud S, Muller G, Moore EG, et al. Brilliant Sm, Eu, Tb, and Dy chiral lanthanide complexes with strong circularly polarized luminescence. *J Am Chem Soc*. 2007;129(1):77-83. https://doi.org/10.1021/ja064902x

32. Carter RC, Miller CE, Palmer RA, May PS, Metcalf DH, Richardson FS. Circularly polarized luminescence (CPL) spectra of samarium (III) in trigonal Na_3[Sm (oxydiacetate)$_3$]·2$NaClO_4$·6H_2O. *Chem Phys Lett*. 1986;131(1-2):37-43. https://doi.org/10.1016/0009-2614(86)80513-9

33. May PS, Metcalf DH, Richardson FS, Carter RC, Miller CE, Palmer RA. Measurement and analysis of excited-state decay kinetics and chiroptical activity in the 6HJ ← 4G52 transitions of Sm3+ in trigonal $Na_3[Sm(C_4H_4O_5)_3]$ 2$NaClO_4$ 6H_2O. *J Lumin*. 1992;51(5):249-268. https://doi.org/10.1016/0022-2313(92)90076-L

34. Carter RC, Metcalf DH, Miller CE, et al. CPL of Sm (III): comparison of experimental and calculated emission (CPL and TL) spectra of $Na_3[Sm(ODA)_3]$·2$NaClO_4$·6H_2O. *J Common Met*. 1986;126:303. https://doi.org/10.1016/0022-5088(86)90309-7

35. Górecki M, Carpita L, Arrico L, Zinna F, Bari LD. Chiroptical methods in a wide wavelength range for obtaining ln 3+ complexes with circularly polarized luminescence of practical interest. *Dalton Trans*. 2018;47(21):7166-7177. https://doi.org/10.1039/C8DT00865E

36. Kreidt E, Arrico L, Zinna F, Bari LD, Seitz M. Circularly polarised luminescence in enantiopure samarium and europium cryptates. *Chem Eur J*. 2018;24(51):13556-13564. https://doi.org/10.1002/chem.201802196

37. Bünzli J-CG. Lanthanide luminescence for biomedical analyses and imaging. *Chem Rev*. 2010;110(5):2729-2755. https://doi.org/10.1021/cr900362e

38. Harada T, Hasegawa Y, Nakano Y, et al. Circularly polarized luminescence from chiral Eu (III) complex with high emission quantum yield. *J Alloys Compd*. 2009;488(2):599-602. https://doi.org/10.1016/j.jallcom.2008.09.100

39. Kroupa DM, Brown CJ, Heckman LM, Hopkins TA. Chiroptical study of chiral discrimination by amino acid based ionic liquids. *J Phys Chem B*. 2012;116(16):4952-4958. https://doi.org/10.1021/jp300357z

40. Hanwell MD, Curtis DE, Lonie DC, Vandermeersch T, Zurek E, Hutchison GR. Avogadro: an advanced semantic chemical editor, visualization, and analysis platform. *J Chem*. 2012;4(1):17. https://doi.org/10.1186/1758-2946-4-17

41. Schmidt MW, Baldridge KK, Boatz JA, et al. General atomic and molecular electronic structure system. *J Comput Chem*. 1993;14(11):1347-1363. https://doi.org/10.1002/jcc.540141112

42. Bode BM, Gordon MS. Macmolplt: a graphical user interface for GAMESS. *J Mol Graph Model*. 1998;16(3):133-138. https://doi.org/10.1016/S1093-3263(99)00002-9

43. Humphrey W, Dalke A, Schulten K. VMD: visual molecular dynamics. *J Mol Graph*. 1996;14(1):33-38. https://doi.org/10.1016/0263-7855(96)00018-5

44. Stewart JJP. Optimization of parameters for semiempirical methods I. Method. *J Comput Chem*. 1989;10(2):209-220. https://doi.org/10.1002/jcc.540100208

45. Stewart JJP. Optimization of parameters for semiempirical methods II. Applications. *J Comput Chem*. 1989;10(2):221-264. https://doi.org/10.1002/jcc.540100209

46. Ditchfield R, Hehre WJ, Pople JA. Self-consistent molecular-orbital methods. IX. An extended Gaussian-type basis for molecular-orbital studies of organic molecules. *J Chem Phys*. 1971;54(2):724-728. https://doi.org/10.1063/1.1674902

47. Hehre WJ, Ditchfield R, Pople JA. Self—consistent molecular orbital methods. XII. Further extensions of Gaussian—type basis sets for use in molecular orbital studies of organic molecules. *J Chem Phys*. 1972;56(5):2257-2261. https://doi.org/10.1063/1.1677527

48. Francl MM, Pietro WJ, Hehre WJ, et al. Self-consistent molecular orbital methods. XXIII. A polarization-type basis set for second-row elements. *J Chem Phys*. 1982;77(7):3654-3665. https://doi.org/10.1063/1.444267

49. Hariharan PC, Pople JA. The influence of polarization functions on molecular orbital hydrogenation energies. *Theor Chim Acta*. 1973;28(3):213-222. https://doi.org/10.1007/BF00533485

50. Cundari TR, Stevens WJ. Effective core potential methods for the lanthanides. *J Chem Phys*. 1993;98(7):5555-5565. https://doi.org/10.1063/1.464902

51. Clark T, Chandrasekhar J, Spitznagel GW, Schleyer PVR. Efficient diffuse function-augmented basis sets for anion calculations. III. The 3-21+G basis set for first-row elements, Li–F. *J Comput Chem*. 1983;4(3):294-301. https://doi.org/10.1002/jcc.540040303

52. Samikkanu S, Mellem K, Berry M, May PS. Luminescence properties and water coordination of Eu3+ in the binary solvent mixture water/1-butyl-3-methylimidazolium chloride. *Inorg Chem*. 2007;46(17):7121-7128. https://doi.org/10.1021/ic070329m

53. Holz RC, Chang CA, Horrocks WD. Spectroscopic characterization of the europium (III) complexes of a series of N,N′-Bis (carboxymethyl) macrocyclic ether bis (lactones). *Inorg Chem*. 1991;30(17):3270-3275. https://doi.org/10.1021/ic00017a010

54. Perlmutter-Hayman B. Cooperative binding to macromolecules. A formal approach. *Acc Chem Res*. 1986;19(3):90-96. https://doi.org/10.1021/ar00123a005

55. Takats J, Zhang XW, Day VW, Eberspacher TA. Synthesis and structure of bis[hydrotris(3,5-dimethylpyrazolyl)borato]samarium (II), Sm[HB(3,5-Me2pz)3]2, and the product of its reaction with azobenzene. *Organometallics*. 1993;12(11):4286-4288. https://doi.org/10.1021/om00035a011

56. Click DR, Scott BL, Watkin JG. Highly electrophilic lanthanide complexes containing fluorinated amido ligands: multiple Ln⋯F interactions, agostic interactions and η^6-arene coordination. *Chem Commun*. 1999;0(7):633-634. https://doi.org/10.1039/A809275C

57. Petrovskaya TV, Fedyushkin IL, Bochkarev MN, Shumann G, Veimann R. Synthesis and crystal structure of the Sm (ButNCHCHNBut)2(Bpy) complex. *Russ Chem Bull*. 1997;46(10):1766-1768. https://doi.org/10.1007/BF02495133

58. Hillier AC, Zhang, Maunder GH, et al. Synthesis and structural comparison of a series of divalent ln $(Tp^{R,R'})_2$ (Ln = Sm, Eu, Yb) and trivalent Sm $(Tp^{Me}{}_2)_2X$ (X = F, Cl, I, BPh_4) complexes. *Inorg Chem*. 2001;40(20):5106-5116. https://doi.org/10.1021/ic010325w

59. Koster GF, Dimmock JD, Wheeler RG, Statz H. *Properties of the Thirty Two Point Groups*. Cambridge, MA: MIT Press; 1969.

SUPPORTING INFORMATION

Additional supporting information may be found online in the Supporting Information section at the end of the article.

How to cite this article: Cotter D, Dodder S, Klimkowski VJ, Hopkins TA. Circularly polarized luminescence of Sm (III) and Eu (III) complexes with chiral ligand (*R*/*S*)-BINAPO. *Chirality*. 2019;1-11. https://doi.org/10.1002/chir.23056